

Electrochemical and Photophysical Study of Homoleptic and Heteroleptic Methylated Ru(II) Bis-terpyridine Complexes

Mira T. Rupp,^[a, b] Thomas Auvray,^[a] Garry S. Hanan,^{*,[a]} and Dirk G. Kurth^{*,[b]}

In this study, we investigate the impact of *N*-methylation on the electronic and photophysical properties of both homoleptic and heteroleptic Ru(II) bis-terpyridine complexes based on the recently reported ligand 4'-(4-bromophenyl)-4,4''':4'',4''''-dipyridinyl-2,2':6',2''-terpyridine (Bipytpy), with pyridine substituents in the 4- and 4''-position. The first reduction of the methylated complexes takes place at the pyridinium site and is observed as multi-electron process. Following *N*-methylation, the complexes exhibit higher luminescence quantum yields and longer excited-state lifetimes. Interestingly, the photophysical properties of the heteroleptic and homoleptic complexes are rather

similar. TD-DFT calculations support the experimental results. Furthermore, the complexes are tested as photosensitizers for photocatalytic hydrogen production, as the parent complex **1** [Ru(Bipytpy)(Tolyltpy)](PF₆)₂ (Tolyltpy: 4'-tolyl-2,2':6',2''-terpyridine) was recently shown to be active and highly stable under photocatalytic conditions. However, the methylated complexes reported herein are inactive as photosensitizers under the chosen conditions, presumably due to loss of the methyl groups, converting them to the non-methylated parent complexes.

Introduction

Due to their high affinity to many transition metal ions, terpyridines (2,2':6',2''-terpyridines) have been widely studied in supramolecular chemistry and material sciences.^[1] They can be used as building blocks in supramolecular assemblies such as coordination polymers or metal organic frameworks.^[1a,2] With group 8 metals, they form kinetically stable *d*⁶ complexes with a distorted octahedral geometry, which show reversible redox behavior as well as a strong absorption in the visible region.^[3] The electrochemical and photophysical properties of these complexes can be tuned by introducing electron-withdrawing or electron-accepting substituents.^[4] Constable and coworkers have previously published several studies regarding *N*-alkylation of ruthenium, iron and osmium bis-terpyridine complexes and their application as photosensitizers in water oxidation as well as molecular switches.^[5] For all investigated complexes, the *N*-

alkylation was introduced at a pyridine ring in the 4'-position of the terpyridine. By introducing different *N*-substituents, they could alter the solubility of the complexes depending on the counter ion as well as the redox behavior and the photophysical properties such as absorption and emission wavelengths and excited-state lifetimes.

In this study, we investigate the effect of *N*-methylation on pyridine substituents in the 4'''- and 4''''-position of the ligand 4'-(4-bromophenyl)-4,4''':4'',4''''-dipyridinyl-2,2':6',2''-terpyridine (Bipytpy). This ligand was used to prepare complex **1** [Ru(Tolyltpy)(Bipytpy)]²⁺ (Tolyltpy: 4'-tolyl-2,2':6',2''-terpyridine), which has been recently reported by our group to be a capable photosensitizer in photocatalytic hydrogen evolution.^[4a] Based on those observations, we were interested in the potential positive impact of structural variation on the performance in photocatalysis. We thus investigate here the effect of a homoleptic vs. heteroleptic design. The structures of the complexes **1** to **4** discussed in this study are shown in Figure 1.

[a] M. T. Rupp, Dr. T. Auvray, Prof. Dr. G. S. Hanan
Département de Chimie
Université de Montréal
1375 Avenue Thérèse-Lavoie-Roux, Montréal, Québec, H2V-0B3, Canada
E-mail: garry.hanan@umontreal.ca

[b] M. T. Rupp, Prof. Dr. D. G. Kurth
Chemische Technologie der Materialsynthese
Julius-Maximilians-Universität Würzburg
Röntgenring 11, 97070 Würzburg, Germany
E-mail: dirk.kurth@matsyn.uni-wuerzburg.de

Supporting information for this article is available on the WWW under <https://doi.org/10.1002/ejic.202100092>

© 2021 The Authors. European Journal of Inorganic Chemistry published by Wiley-VCH GmbH. This is an open access article under the terms of the Creative Commons Attribution Non-Commercial NoDerivs License, which permits use and distribution in any medium, provided the original work is properly cited, the use is non-commercial and no modifications or adaptations are made.

Results and Discussion

Synthesis and structural analysis

The synthesis of the ligands as well as of complex **1** has been described previously.^[4a] The homoleptic complex **2** is synthesized in a one-step procedure, reacting two equivalents of the ligand Bipytpy with a Ru(III) chloride salt using microwave irradiation. Both the heteroleptic and the homoleptic complexes **1** and **2** are then methylated using iodomethane, followed by addition of aqueous potassium hexafluorophosphate to isolate the complexes **3** and **4** as PF₆⁻ salts. Their identity is confirmed by ¹H and ¹³C NMR analysis (Figures S.I. 1–6) and ESI-MS.

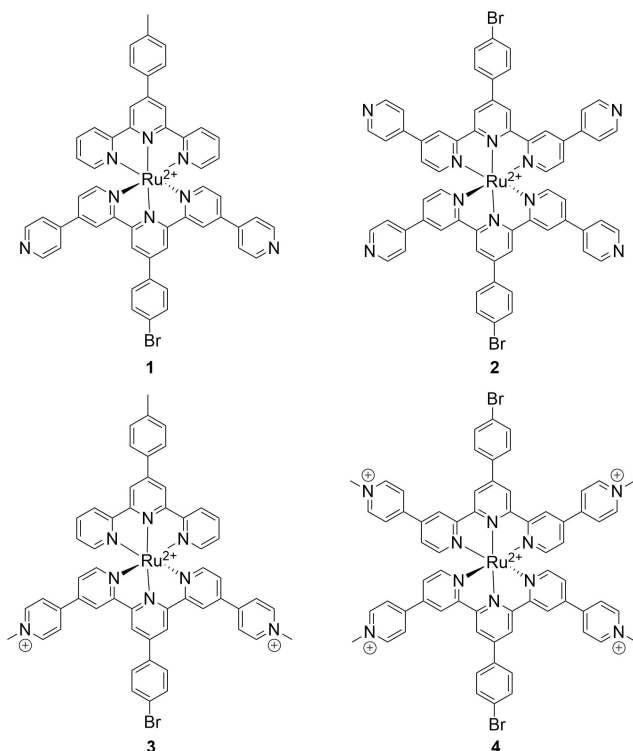


Figure 1. Structures of the complexes 1 to 4 discussed in this paper.

Single crystals of complexes 2 and 3 are obtained either by slow evaporation of an acetonitrile/water solution for complex 2 or slow diffusion of diethyl ether into a concentrated acetonitrile solution of the complex 3. The crystals are analyzed using X-ray diffraction. The structures are shown in Figure 2 with refinement parameters described in the SI. In both complexes, the ruthenium cation has a distorted octahedral coordination sphere, resulting from the restricted bite angle of the two meridionally coordinated terpyridine ligands. The crystal structure analysis confirms the expected structures of the complexes.

Electrochemical properties

The electrochemical properties of complexes 1 to 4 are investigated using cyclic voltammetry in deaerated acetonitrile. The experimental setup is described in the SI. The cyclic voltammograms of the anodic and cathodic scan conducted in one single experiment are shown in Figure 3. Cyclic voltammograms of both anodic and cathodic scan conducted in one single experiment are shown in Figure S.I. 7. The potentials are reported vs. ferrocene (Fc/Fc^+) as a reference. All complexes exhibit a reversible oxidation, which takes place at the metal center.^[3a,6] The non-methylated and methylated homoleptic complexes 2 and 4 are harder to oxidize, i.e., the oxidation potential is shifted anodically by +50–100 mV, with respect to the corresponding heteroleptic complexes 1 and 3. This shift in oxidation potentials can be explained by the absence of an electron-donating ligand in the

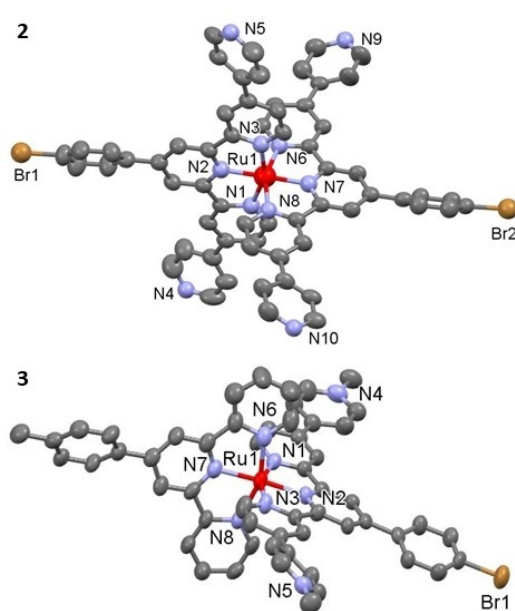


Figure 2. Ellipsoid representation of complexes 2 and 3 at 50% probability. Hydrogen atoms, PF_6^- counterions and co-crystallized solvent molecules are omitted for clarity.

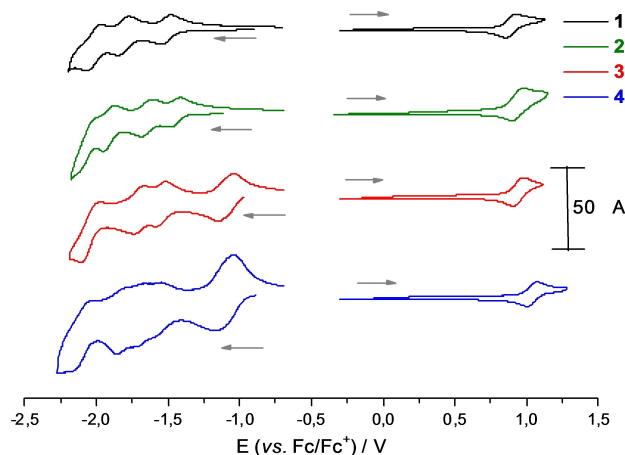


Figure 3. Cyclic voltammograms of complexes 1 to 4 (0.5 mM) in dry acetonitrile under inert gas atmosphere, with 0.1 M TBAPF_6 ; scan rate 100 mV/s; scans both in anodic and cathodic direction start at 0 V vs. reference.

homoleptic complexes, i.e., the electron-donating tolyl substituent in the heteroleptic complexes destabilizes the metal-centered HOMO and thus facilitates the oxidation of the Ru(II) center while the electron-accepting pyridine and *N*-methyl pyridinium substituents slightly stabilize the HOMO.^[6] The homoleptic complex $[\text{Ru}(\text{Tolytpty})_2]^{2+}$ exhibits an oxidation potential of 0.84 V vs. Fc/Fc^+ and is thus slightly easier to oxidize than complex 1 with an oxidation potential of 0.89 V.^[7] This anodic shift is assumed to be due to the HOMO destabilizing effect of the electron-donating Tolytpty ligand,

which is less pronounced in the heteroleptic complex **1**. A similar anodic shift in oxidation potentials can also be observed comparing the non-methylated complexes **1** and **2** with their methylated counterparts **3** and **4**. The methylation of the pyridine substituents makes the ligands electron poorer and thus more electron-withdrawing, resulting in a stronger stabilization of the metal-centered HOMO and therefore an anodic shift of the oxidation potential. This observation matches well with the results reported by Constable *et al.* on related *N*-methylated and *N*-alkylated ruthenium bis-terpyridine complexes.^[5b,8]

The non-methylated complexes **1** and **2** exhibit three reversible reduction processes in the investigated window, which take place at the ligands. The methylated complexes **3** and **4** both show one reversible reduction process (or several very close lying processes) taking place at -1.1 V vs. Fc/Fc^+ . In the case of complex **3**, this first reduction is a two-electron process, determined by square wave voltammetry (Figure S.I. 10), while in the case of complex **4**, it is a four-electron process (Figure S.I. 11). The first reduction of the methylated complexes presumably takes place at the pyridinium ions, indicated both by the multiple electron processes as well as the strongly anodically shifted reduction potential.^[5b] The strong anodic shift of these redox processes again matches well with a study conducted by Constable and Cargill Thompson. However, in a homoleptic ruthenium bis-terpyridine complex with *N*-methylated pyridine substituents, they observed two separate reductions of the pyridinium sites.^[5b] Their observation supports the assumption that the processes observed around -1.1 V for complexes **3** and **4** are indeed multiple, overlapping one-electron processes, which also explains the large peak separation (> 100 mV). Complexes **3** and **4**, furthermore, show three and four reversible reduction processes in the investigated window, respectively. We previously assigned the reductions occurring in complex **1** by comparison with the homoleptic $[\text{Ru}(\text{Tolyltpy})_2]^{2+}$ complex, leading to the following assignment: The first reduction process corresponds to a first reduction of the pyridine substituted ligand; the second reduction process corresponds to a first reduction of the Tolyltpy ligand; the third reduction process corresponds to a second reduction process of the pyridine substituted ligand.^[4a] Following this assignment, we assume that in complex **3**, the reductions occurring at -1.55 V and -2.04 V vs. Fc/Fc^+ correspond to a first and second reduction of the electron-withdrawing pyridinium substituted ligand while the reduction process at -1.70 V occurs at the Tolyltpy ligand. In the homoleptic complex **2**, four reduction processes are observed in the investigated window. These

Table 1. Electrochemical half-wave redox potentials $E_{1/2}$ in V ($\Delta E_p/\text{mV}$) for complexes **1** to **4** in inert-gas purged acetonitrile.^[a]

	Oxidation $E_{1/2}$ / V	Reduction $E_{1/2}$ / V			
1	0.89 (69)	-1.51 (62)	-1.81 (75)	-2.02 (104)	
2	0.94 (69)	-1.45 (61)	-1.64 (61)	-1.92 (83)	-2.06 (98)
3	0.94 (71)	-1.10 (102)	-1.55 (62)	-1.70 (71)	-2.04 (139)
4	1.04 (73)	-1.11 (114)	-1.58 (66)	-1.69 (70)	-1.82 (84) -2.09 (142)

[a] Redox potentials are reported vs. ferrocene (Fc/Fc^+); the differences between the cathodic and anodic peak potentials ΔE_p are given in parentheses in millivolts; measurements are carried out in deaerated acetonitrile solutions containing 0.1 M tetrabutylammonium hexafluorophosphate at a scan rate of 100 mV s^{-1} .

correspond to both ligands being reduced twice. Complex **4** exhibits four reduction processes below -1.5 V, which correspond to each ligand being reduced twice. The data are summarized in Table 1.

Photophysical properties

The complexes are analyzed regarding their photophysical properties in acetonitrile. The UV-vis absorption and emission spectra are presented in Figure 4, the data are summarized in Table 2. All complexes exhibit metal-to-ligand charge transfer (MLCT) absorption bands around 500 nm, with absorption maxima slightly red-shifted for the homoleptic complexes **2** and **4** compared to their heteroleptic counterparts. The methylated complexes **3** and **4** exhibit a broader, red-shifted MLCT absorption band, with lower absorptivity compared to the non-methylated analogues. These broader absorption bands overlap with other transitions at higher energy (around 400 nm), which are presumably ligand-centered (LC) transitions. Additionally, complex **3** exhibits a shoulder around 470 nm, which is attributed to a MLCT transition, likely involving mainly the Tolyltpy ligand, based on the higher energy of this transition.

Regarding the emission wavelength, the methylated complexes **3** and **4** again exhibit a red-shifted (25–40 nm) emission compared to the non-methylated complexes **1** and **2**. Furthermore, the quantum yield of the methylated complexes as well as their excited-state lifetime are increased by an order of magnitude compared to complexes **1** and **2**. Additionally, the homoleptic complexes **2** and **4** also exhibit a blue-shifted

Table 2. UV-vis absorption and emission data of complexes **1** to **4**; spectra measured in acetonitrile.^[a]

	$\lambda_{\text{abs,max}}/\text{nm}$ ($\epsilon/10^3 \text{ L mol}^{-1} \text{ cm}^{-1}$)				$\lambda_{\text{em,max}}/\text{nm}$	$\Phi/10^{-5}$	τ/ns
1	233 (92)	302 (80)	332 (70)	497 (34)	658	74 ± 33	3.8 ± 0.5
2	235 (100)	296 (63)	332 (70)	502 (30)	649	78 ± 32	2.4 ± 0.2
3	228 (95)	275 (77)	309 (65)	408 (15)	511 (21)	295 ± 128	36 ± 1
4	238 (77)	265 (80)	307 (44)	344 (46)	377 (19) 519 (22)	405 ± 160	39 ± 1

[a] Maximum absorption wavelength $\lambda_{\text{abs,max}}$, extinction coefficient ϵ , maximum emission wavelength $\lambda_{\text{em,max}}$, luminescence quantum yield Φ , excited-state lifetime τ ; emission data is collected in inert-gas purged solutions at room temperature.

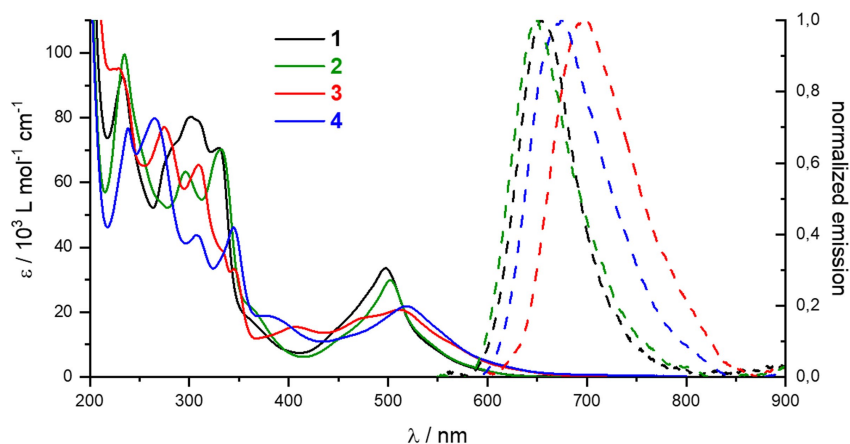


Figure 4. UV-vis absorption spectra (solid lines) and normalized emission spectra (dashed lines) of complexes 1 to 4; spectra measured in acetonitrile.

emission compared to the heteroleptic complexes 1 and 3. We assume this observation is due to the lack of the electron-donating Tolytpy ligand in the homoleptic complexes. The electron-donating character of the Tolytpy ligand leads to a destabilization of the HOMO and thus to a smaller HOMO-LUMO energy gap,^[4c] i.e., a red-shifted emission wavelength.

A study by Constable and coworkers on *N*-alkylated 4'-pyridyl substituted bis-terpyridine complexes yielded similar quantum yields around 40×10^{-4} . However, the observed excited-state lifetimes of these complexes were found to be increased by a factor of 3–4 compared to the herein reported complexes and the emission wavelengths to be red-shifted to around 720 nm.^[8] A longer excited-state lifetime despite a lower HOMO-LUMO energy gap, as indicated by the emission wavelength, indicates that the non-radiative decay is not governed by direct deactivation from the excited-state to the ground state and can hence not be described by the energy gap law, but rather involves the triplet metal-centered (³MC) state. Assuming that the energy of the ³MC state is less affected than the ³MLCT state by the more electron-withdrawing character of the ligands due to methylation, a stronger red-shift of the emission wavelength of the complexes reported by Constable *et al.* indicates a larger ³MLCT to ³MC energy gap and hence a less efficient deactivation of the excited state, resulting in longer excited-state lifetimes.

Theoretical calculations

To further understand the observations in the photophysical and electrochemical experiments and to support our conclusions, we conducted theoretical calculations using density functional theory (DFT) and time-dependent DFT (TD-DFT). Figure 5 shows the calculated HOMO and LUMO energies of the four complexes 1 to 4. The LUMO energies of the methylated complexes 3 and 4 are significantly lower than those of the non-methylated complexes 1 and 2. This shift in energy

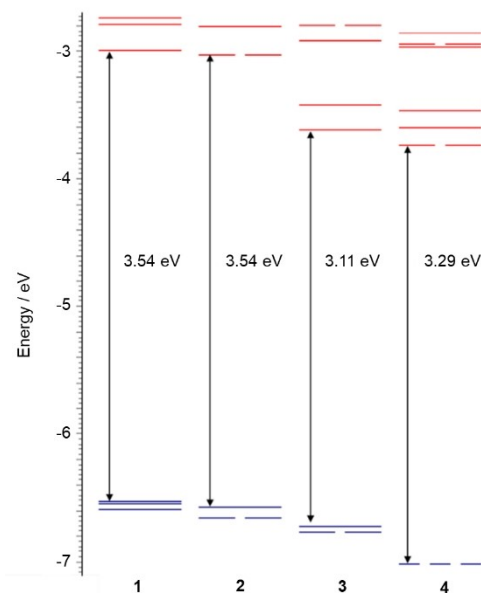


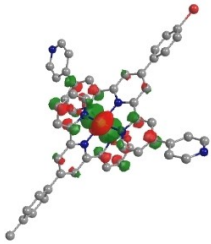
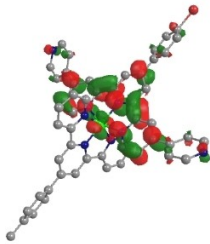
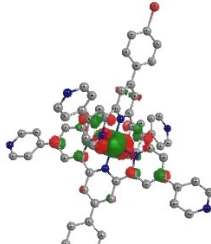
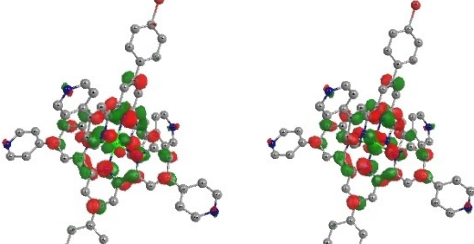
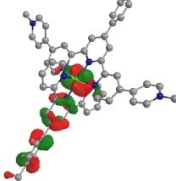
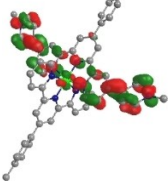
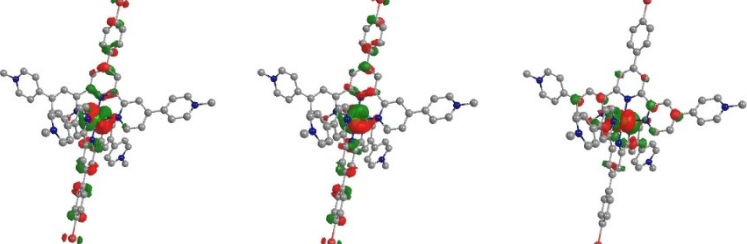
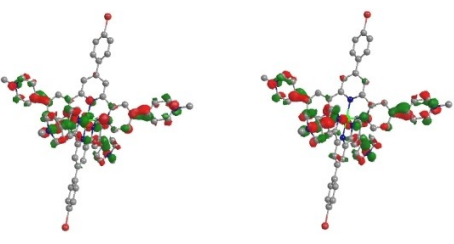
Figure 5. Energy diagram of the frontier orbitals of the Ru(II) complexes 1 to 4 (degeneracy threshold of 15 meV).

matches well the observed anodically shifted reduction potentials of complexes 3 and 4.

Furthermore, HOMOs of the homoleptic complexes 2 and 4 are stabilized compared to the heteroleptic complexes 1 and 3. This effect is stronger for the methylated complexes, presumably due to the more electron-withdrawing character of the methylated ligand. The strong stabilization of the HOMO of complex 4 leads to a larger calculated HOMO-LUMO gap in comparison to complex 3. The larger energy gap agrees with the observed higher energy emission wavelength (Table 2).

The impact of the homoleptic vs. the heteroleptic design of the complexes can further be visualized when looking at the calculated contributions to the molecular orbitals (MOs). Table 3

Table 3. Contributions to MOs for complexes 1 to 4.

	HOMO	LUMO
1	 <p>–6.53 eV Ru: 66% Tolytpty: 15%; Bipytpy: 19%</p>	 <p>–3.00 eV Ru: 7% Tolytpty: 1%; Bipytpy: 92%</p>
2	 <p>–6.58 eV Ru: 64% Bipytpy: 36%</p>	 <p>–3.03 eV Ru: 7% Bipytpy: 93%</p> <p>–3.03 eV Ru: 7% Bipytpy: 93%</p>
3	 <p>–6.73 eV Ru: 52% Tolytpty: 32%; Me-Bipytpy: 16%</p>	 <p>–3.62 eV Ru: 4% Tolytpty: 3%; Me-Bipytpy: 93%</p>
4	 <p>–7.02 eV Ru: 55% Me-Bipytpy: 45%</p> <p>–7.02 eV Ru: 56% Me-Bipytpy: 44%</p> <p>–7.03 eV Ru: 65% Me-Bipytpy: 35%</p>	 <p>–3.74 eV Ru: 4% Me-Bipytpy: 96%</p> <p>–3.74 eV Ru: 4% Me-Bipytpy: 96%</p>

shows the calculated distribution of the electron density in the HOMOs and LUMOs of complexes 1 to 4. The electron density in the HOMO is localized mainly on the ruthenium center for all four complexes. In the case of complex 4, the HOMO is described by three degenerated states. As expected, the electron density in the LUMO is centered on the terpyridine moieties. In heteroleptic complexes 1 and 3, most of the electron density is on the pyridine-substituted ligand, in agreement with its more electron-withdrawing nature. This non-

symmetrical electron density in the LUMO of complexes 1 and 3 is expected due to the heteroleptic design. In contrast, for the homoleptic complexes 2 and 4, two degenerate states exist, with the electron density delocalized equally over both ligands. The methylation of the peripheral pyridine substituents increases the contribution of these rings to the LUMO levels, in agreement with the pyridinium centered reduction observed in the electrochemical measurements.

TD-DFT calculations provide insight into the nature of the excited state of the reported complexes. The singlet-triplet transition corresponding to the excited state are presented in Table S.I. 3. In all cases, they correspond to MLCT states mixed with minor contributions of LC states. While the methylation in complexes **3** and **4** extends the delocalization on the Bipytpy ligand towards the pyridines in the 4'''- and 4''''-position, the pyridine rings have no or only a minor contribution in the excited state with no contribution from the methyl groups, similarly to what Constable and coworkers had observed for their system.^[8]

Photocatalytic study for hydrogen evolution

We previously reported that complex **1** acts as photosensitizer (PS) in hydrogen evolution experiments, exhibiting relatively weak, yet very long lasting activity.^[4a] The complexes discussed in this paper are tested under similar catalytic conditions, using the catalyst $[\text{Co}(\text{dmgH})_2(\text{H}_2\text{O})_2](\text{BF}_4)_2$, prepared *in-situ* from $[\text{Co}(\text{H}_2\text{O})_6](\text{BF}_4)_2$ (1 mM) and dmgH_2 (6 mM), or colloidal platinum, prepared *in-situ* from K_2PtCl_4 , as reported in other photocatalytic studies.^[4a,b] The tests are conducted in DMF with 1 M triethanolamine (TEOA) as sacrificial electron donor and 0.1 M tetrafluoroboric acid (HBF_4) as proton source. The instrumental error of the reported values is found to be within 10%. Results are reported in turn-over frequency (TOF) and turn-over number (TON). Complex **2** is active as photosensitizer both with the cobaloxime complex or the colloidal platinum used as catalyst (Figure 6 and Figure S.I. 16). However, its activity as well as stability are inferior to that of the previously reported heteroleptic complex **1** (Figure 6). Complex **1** has been reported to be active as PS for more than 12 days without reaching its half-life time ($\text{TOF}_{\text{max}} = 56 \text{ mmol}_{\text{H}_2} \text{ mol}_{\text{PS}}^{-1} \text{ min}^{-1}$).^[4a] Complex **2**

on the other hand exhibits a half-life time of 5.2 h and a TOF_{max} of $36 \text{ mmol}_{\text{H}_2} \text{ mol}_{\text{PS}}^{-1} \text{ min}^{-1}$ when using a cobaloxime catalyst and a TOF_{max} of $35 \text{ mmol}_{\text{H}_2} \text{ mol}_{\text{PS}}^{-1} \text{ min}^{-1}$ with a half-life time of 8.0 h using colloidal platinum. Yet, the UV-vis absorption spectra of the reaction mixtures recorded before and after blue light irradiation only vary very slightly (see Figure S.I. 17), which shows that complex **2** does not decompose during the hydrogen evolution reaction and that other components of the system lead to the loss of hydrogen production activity over time. Previously, we argued that the relatively low hydrogen evolution activity of PS **1** is a result of the reductive quenching being the rate limiting step.^[4a] The fact, that the activity as PS of complex **2** is very similar regardless of the catalyst used indicates that here too, the rate limiting step does not involve the catalyst. However, complex **2** is slightly easier to reduce, which should make the reductive quenching more efficient and hence increase the activity in hydrogen evolution experiments. The fact that instead of an increased activity rather a lower activity and decreased longevity of hydrogen production is observed with complex **2** compared to complex **1**, leads to the conclusion that the heteroleptic design of complex **1**, leading to a non-symmetrical electron density distribution in the excited state, is beneficial for the electron transfer processes. However, more detailed studies are needed to further investigate this effect.

Despite its improved photophysical properties, only very low activity is observed from complex **3** using a cobalt-based catalyst ($\text{TOF}_{\text{max}} = 22 \text{ mmol}_{\text{H}_2} \text{ mol}_{\text{PS}}^{-1} \text{ min}^{-1}$, see Figure 6). In contrast, using colloidal Pt as catalyst, the methylated complex **3** shows an unusual activity profile where the hydrogen production starts very slow and increases over time reaching a TOF_{max} of $45 \text{ mmol}_{\text{H}_2} \text{ mol}_{\text{PS}}^{-1} \text{ min}^{-1}$ (Figure S.I. 16). UV-vis absorption spectra recorded before and after the experiment (Figure S.I.8) suggest that the complex is not stable under the catalytic conditions. The UV-vis absorption spectra after the hydrogen evolution experiments show an absorption profile very similar to that of complex **1**, leading to the assumption that complex **3** is demethylated. Interestingly, the absorption profiles of the reaction mixtures after irradiation with light differ slightly depending on which catalyst is used. While the reaction mixture containing a cobaloxime catalyst leads to a spectrum identical to that of complex **1**, the reaction mixture with colloidal platinum differs slightly, with a small bathochromic shift of the MLCT absorption band. These small differences in absorbance are also reflected in the hydrogen evolution activity, i.e., only with colloidal platinum, the decomposition product leads to hydrogen evolution activity. It should, however, be noted that different batches of freshly *in-situ* prepared colloidal platinum can lead to slightly varying hydrogen evolution profiles, albeit exhibiting similar TOF_{max} . When a cobaloxime catalyst is used, a maximum TOF_{max} of $22 \text{ mmol}_{\text{H}_2} \text{ mol}_{\text{PS}}^{-1} \text{ min}^{-1}$, with a half-life time of 2.9 h is found. We assume that the cobaloxime catalyst is participating in the demethylation reaction, rendering it inactive for the hydrogen evolution reaction.

Complex **4** is found to be not active as PS, both with the cobaloxime and the colloidal platinum catalyst. Again, UV-vis

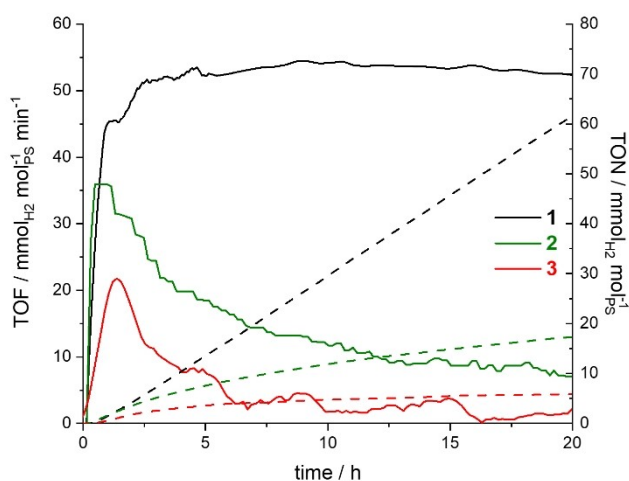


Figure 6. Hydrogen photoproduction with complexes **1**, **2** and **3** as PS (0.1 mM) under blue light irradiation (LED centered at 445 nm); with $[\text{Co}(\text{H}_2\text{O})_6](\text{BF}_4)_2$ as pre-catalyst (1 mM), with dmgH_2 (6 mM), TEOA as sacrificial electron donor (1 M) and HBF_4 as proton source (0.1 M) in DMF; TOF: solid lines; TON: dashed lines.

absorption spectra of the reaction mixtures recorded before and after light irradiation show a change in the absorption profile. This change could either stem from a decomposition, such as demethylation, or reduction of the complex. We propose that, due to the less negative reduction potentials of the methylated complexes **3** and **4**, they are easily reduced by the sacrificial electron donor, but the reduced species lack driving force to subsequently transfer the electron to the catalyst. While the cyclic voltammograms show that the reduction processes are reversible, the catalytic conditions (light irradiation and presence of other reagents) apparently lead to a decomposition of the methylated complexes **3** and **4**, e.g., *via* loss of the methyl groups.

Conclusion

In this study, we compare the previously reported heteroleptic complex **1** with its homoleptic counterpart **2** and prepare the corresponding methylated complexes **3** and **4**. Comparing the homoleptic and heteroleptic complexes, we find that the homoleptic complexes **2** and **4** are harder to oxidize but easier to reduce. As expected, the first reduction of the methylated complexes **3** and **4** takes place at the pyridinium site and is observed as multi-electron process. Furthermore, the photo-physical properties are barely affected by changing from heteroleptic **1** to homoleptic **2**. Both methylated complexes exhibited higher luminescence quantum yields and longer excited-state lifetimes. Photocatalytic investigations show that methylation of the complexes makes them unsuitable for the application as PS in hydrogen evolution experiments. This observation is assumed to be due to decomposition, e.g., *via* loss of the methyl groups, under the catalytic conditions and a lack of driving force for electron transfer from the reduced PS to the catalyst. However, the anodically shifted oxidation potentials of the methylated complexes could render these complexes interesting candidates for photosensitizers in photocatalytic water oxidation. In catalytic systems for water oxidation, the excited PS is usually oxidized by a sacrificial electron acceptor, yielding a Ru(III) species. Compounds similar to the methylated complexes **3** and **4**, i.e., *N*-alkylated 4'-pyridyl substituted terpyridine ruthenium complexes, were previously studied as photosensitizers in photocatalytic water oxidation. These studies showed that the *N*-alkylated bis-terpyridine complexes can lead to a comparable oxygen evolution activity as the standard ruthenium tris-terpyridine PS.^[5]

Experimental Section

Materials All reagents and solvents were obtained from commercial sources (VWR, Fisher Scientific, Acros or Sigma Aldrich) and used as received, unless stated otherwise. RuCl₃·3H₂O was obtained from Pressure Chemicals Inc. The synthesis of the ligands Tolytpy^[9] and Bipytpy^[4a] were carried out according to published procedures. The synthesis of the complex [Ru(Tolytpy)(Bipytpy)]²⁺ **1** was carried out as a two-step procedure as described previously.^[4a] For experiments

under microwave irradiation, a Biotage Initiator or a Discover SP microwave synthesizer were used.

Synthesis [Ru(Bipytpy)]₂(PF₆)₂ **2** A suspension of Ru(III) chloride trihydrate (11.8 mg, 45.0 μmol, 1 eq) and Bipytpy (50.0 mg, 92.2 μmol, 2.05 eq) in 7.00 mL ethylene glycol was heated to 150 °C for 40 minutes using microwave irradiation. After cooling to room temperature, water and aqueous KPF₆ solution were added to the solution and the precipitate was filtered off over celite. After washing with water, the solid was dissolved in acetonitrile, dried over magnesium sulfate and the solvent was removed under reduced pressure. The crude product was purified by washing with dichloromethane to yield the product as a dark red solid (62.0 mg, 42.0 μmol, 93.4%).

¹H-NMR (400 MHz, CD₃CN): δ = 9.24 (s, 4H), 8.99 (s, 4H), 8.77 (d, ³J = 5.7 Hz, 8H), 8.24 (d, ³J = 8.4 Hz, 4H), 8.01 (d, ³J = 8.3 Hz, 4H), 7.79 (d, ³J = 5.6 Hz, 8H), 7.61 (d, ³J = 5.9 Hz, 4H) and 7.54 ppm (d, ³J = 5.7 Hz, 4H). ¹³C{¹H}-NMR (125 MHz, CD₃CN): δ = 159.8, 156.5, 154.0, 151.8, 148.4, 148.3, 143.6, 136.8, 133.7, 130.6, 125.9, 125.6, 123.4, 123.1 and 122.5 ppm. ESI-MS: m/z [M]²⁺ calc. for C₆₂H₄₀Br₂N₁₀Ru: 592.04183; found: 592.04471; difference: 4.9 ppm.

[Ru(Tolytpy)(di-methyl-Bipytpy)](PF₆)₄ **3** To a solution of [Ru(Bipytpy)(Tolytpy)](PF₆)₂ **1** (35.0 mg, 27.9 μmol, 1 eq) in 10.0 mL acetonitrile, iodomethane (79.1 mg, 34.7 μL, 557 μmol, 20 eq) was added. The reaction mixture was stirred at room temperature for 2 h and subsequently heated to 40 °C for two days. During the course of the reaction, additional iodomethane was added. The product was isolated by removal of the solvent and excess iodomethane under vacuum. To exchange the iodide counter ions, the dark red solid was dissolved in acetonitrile and aqueous potassium hexafluorophosphate solution and water were added. The precipitate was filtered off and washed with water (33.3 mg, 21.1 μmol, 75.8%).

¹H-NMR (300 MHz, CD₃CN): δ = 9.25 (s, 2H), 9.04 (m, 4H), 8.76 (d, ³J = 6.4 Hz, 4H), 8.69 (d, ³J = 8.1 Hz, 2H), 8.34 (d, ³J = 6.4 Hz, 4H), 8.23 (d, ³J = 8.4 Hz, 2H), 8.15 (d, ³J = 8.0 Hz, 2H), 7.98 (m, 4H), 7.74 (d, ³J = 5.9 Hz, 4H), 7.61 (d, ³J = 7.4 Hz, 4H), 7.44 (d, ³J = 5.1 Hz, 2H), 7.21 (m, 2H), 4.35 (s, 6H) and 2.56 ppm (s, 3H). ¹³C{¹H}-NMR (75 MHz, CD₃CN): δ = 160.4, 159.1, 156.4, 156.1, 154.4, 153.7, 152.0, 150.3, 148.2, 147.0, 143.7, 143.7, 142.2, 139.5, 136.8, 134.7, 133.8, 131.3, 130.6, 128.7, 128.5, 126.9, 126.5, 125.7, 125.6, 123.7, 123.4, 122.7, 49.2 and 21.4 ppm. ESI-MS: m/z [M]²⁺ calc. for C₅₅H₄₃Br₂N₈Ru: 498.09133; found: 498.0926; difference: 2.6 ppm.

[Ru(di-methyl-Bipytpy)]₂(PF₆)₆ **4** To a solution of [Ru(Bipytpy)]₂(PF₆)₂ **2** (40.0 mg, 27.1 μmol, 1 eq) in 10.0 mL acetonitrile, iodomethane (385 mg, 167 μL, 2.71 mmol, 100 eq) was added. The reaction mixture was heated to reflux for 4 h. The product was isolated by removal of the solvent and excess iodomethane under vacuum. To exchange the iodide counter ions, the dark red solid was dissolved in acetonitrile and aqueous potassium hexafluorophosphate solution and water were added. The precipitate was filtered off and washed with water (41.0 mg, 19.4 μmol, 71.5%).

¹H-NMR (500 MHz, CD₃CN): δ = 9.29 (s, 4H), 9.06 (s, 4H), 8.76 (d, ³J = 6.8 Hz, 8H), 8.33 (d, ³J = 6.8 Hz, 8H), 8.25 (d, ³J = 8.4 Hz, 4H), 8.02 (d, ³J = 8.4 Hz, 4H), 7.74 (d, ³J = 6.0 Hz, 4H), 7.62 (dd, ³J = 6.0 Hz, ⁴J = 1.8 Hz, 4H) and 4.34 ppm (s, 12H). ¹³C{¹H}-NMR (125 MHz, CD₃CN): δ = 160.3, 156.2, 154.8, 151.9, 149.1, 147.0, 144.2, 136.7, 133.8, 130.6, 126.9, 126.6, 125.8, 123.9, 123.7 and 49.2 ppm. ESI-MS: m/z [M + 3H]³⁺ calc. for C₆₆H₅₂Br₂N₁₀Ru: 415.73350; found: 415.72972; difference: 9.1 ppm.

Computational details The calculations were made with Gaussian16 rev.B.01,^[10] using the PBE0 hybrid functional^[11] with LanL2DZ^[12] as basis set. The optimizations were conducted without

symmetry constraints, followed by frequency calculations to confirm that energy minima had been reached in all cases. The energy, oscillator strength, and related MO contributions for the 100 lowest singlet-singlet and 10 lowest singlet-triplet excitations were obtained from the TD-DFT/singlets and the TD-DFT/triplets output files, respectively, for the S_0 -optimized geometry. GaussView6, GaussSum3.3^[13] and Chemissian4.53^[14] were used for data analysis, visualization and surface plots. All calculations were conducted for acetonitrile solvated complexes using a conductor like polarized continuum (CPCM) solvation model.^[15]

Deposition Numbers 2034792 (for 2), and 2034795 (for 3) contain the supplementary crystallographic data for this paper. These data are provided free of charge by the joint Cambridge Crystallographic Data Centre and Fachinformationszentrum Karlsruhe Access Structures service www.ccdc.cam.ac.uk/structures.

Acknowledgements

G.S.H. thanks the Natural Sciences and Engineering Research Council of Canada for financial support. T.A. thanks the Faculté des Arts et Sciences at Université de Montreal for their Marguerite-Jacques-Lemay scholarship. M.T.R. thanks the DAAD for their scholarship for bi-nationally supervised doctoral students. This research was enabled in part by support provided by Compute Canada. Financial support by the BayFor is appreciated by M.T.R. and D.G.K. Open access funding enabled and organized by Projekt DEAL.

Conflict of Interest

The authors declare no conflict of interest.

Keywords: Ruthenium · Luminescence · Electrochemistry · Ligand effects · Photocatalysis

- [1] a) J. Wang, X. Xue, M. Chen, T. Wu, S.-C. Wang, H. Zhao, Z. Jiang, J. Yan, Z. Jiang, Y.-T. Chan, P. Wang, *Inorg. Chem.* **2019**, *58*, 7662–7666; b) T. Mede, M. Jager, U. S. Schubert, *Chem. Soc. Rev.* **2018**, *47*, 7577–7627; c) A. Wild, A. Winter, F. Schlutter, U. S. Schubert, *Chem. Soc. Rev.* **2011**, *40*, 1459–1511.
- [2] a) E. C. Constable, E. L. Dunphy, C. E. Housecroft, M. Neuburger, S. Schaffner, F. Schaper, S. R. Batten, *Dalton Trans.* **2007**, 4323–4332; b) M. Elcheikh Mahmoud, H. Audi, A. Assoud, T. H. Ghaddar, M. Hmadeh, *J. Am. Chem. Soc.* **2019**, *141*, 7115–7121; c) S. Chakraborty, G. R. Newkome, *Chem. Soc. Rev.* **2018**, *47*, 3991–4016; d) S. Pai, M. Moos, M. H. Schreck, C. Lambert, D. G. Kurth, *Inorg. Chem.* **2017**, *56*, 1418–1432; e) G. Schwarz, I. HaBlauer, D. G. Kurth, *Adv. Colloid Interface Sci.* **2014**, *207*, 107–120; f) M. Chen, D. Liu, J. Huang, Y. Li, M. Wang, K. Li, J. Wang, Z. Jiang, X. Li, P. Wang, *Inorg. Chem.* **2019**, *58*, 11146–11154; g) S. Vitale, B. Laramée-Milette, M. E. Amato, G. S. Hanan, N. Tuccitto, A. Licciardello, *Nanoscale* **2019**, *11*, 4788–4793; h) R. Farran, L. Le Quang, D. Jouvenot, F. Loiseau, R. Pansu, A. Deronzier, J. Chauvin, *Inorg. Chim. Acta* **2017**, *454*, 197–207; i) M. K. Bera, Y. Ninomiya, T. Yoshida, M. Higuchi, *Macromol. Rapid Commun.* **2020**, *41*, 1900384; j) M. K. Bera, Y. Ninomiya, M. Higuchi, *ACS Appl. Mater. Interfaces* **2020**, *12*, 14376–14385; k) S. M. Munzert, S. P. Stier, G. Schwarz, H. Weissman, B. Rybtchinski, D. G. Kurth, *Chem. Eur. J.* **2018**, *24*, 2898–2912; l) J. Lombard, D. A. Jose, C. E. Castillo, R. Pansu, J. Chauvin, A. Deronzier, M. N. Collomb, *J. Mater. Chem. C* **2014**, *2*, 9824–9835.
- [3] a) A. Juris, V. Balzani, F. Barigelletti, S. Campagna, P. Belser, A. von Zelewsky, *Coord. Chem. Rev.* **1988**, *84*, 85–277; b) J. P. Sauvage, J. P. Collin, J. C. Chambron, S. Guillerez, C. Coudret, V. Balzani, F. Barigelletti, L. De Cola, L. Flamigni, *Chem. Rev.* **1994**, *94*, 993–1019; c) S. Pai, M. Schott, L. Niklaus, U. Posset, D. G. Kurth, *J. Mater. Chem. C* **2018**, *6*, 3310–3321.
- [4] a) M. Rupp, T. Auvray, E. Rousset, G. M. Mercier, V. Marvaud, D. G. Kurth, G. S. Hanan, *Inorg. Chem.* **2019**, *58*, 9127–9134; b) T. Auvray, R. Sahoo, D. Deschenes, G. S. Hanan, *Dalton Trans.* **2019**, *48*, 15136–15143; c) A. K. Pal, G. S. Hanan, *Chem. Soc. Rev.* **2014**, *43*, 6184–6197; d) Y.-Q. Fang, N. J. Taylor, F. Laverdière, G. S. Hanan, F. Loiseau, F. Nastasi, S. Campagna, H. Nierengarten, E. Leize-Wagner, A. Van Dorsselaer, *Inorg. Chem.* **2007**, *46*, 2854–2863; e) P. Pal, S. Mukherjee, D. Maity, S. Baitalik, *ACS Omega* **2018**, *3*, 14526–14537; f) A. K. Pal, S. Serroni, N. Zaccheroni, S. Campagna, G. S. Hanan, *Chem. Sci.* **2014**, *5*, 4800–4811.
- [5] a) E. C. Constable, A. M. W. C. Thompson, *J. Chem. Soc. Dalton Trans.* **1992**, *24*, 3467–3475; b) E. C. Constable, A. M. W. C. Thompson, *J. Chem. Soc. Dalton Trans.* **1994**, *9*, 1409–1418; c) E. C. Constable, C. E. Housecroft, M. Neuburger, D. Phillips, P. R. Raithby, E. Schofield, E. Sparr, D. A. Tocher, M. Zehnder, Y. Zimmermann, *J. Chem. Soc. Dalton Trans.* **2000**, *13*, 2219–2228; d) J. E. Beves, E. L. Dunphy, E. C. Constable, C. E. Housecroft, C. J. Kepert, M. Neuburger, D. J. Price, S. Schaffner, *Dalton Trans.* **2008**, *3*, 386–396; e) E. C. Constable, C. E. Housecroft, A. C. Thompson, P. Passaniti, S. Silvi, M. Maestri, A. Credi, *Inorg. Chim. Acta* **2007**, *360*, 1102–1110; f) S. Silvi, E. C. Constable, C. E. Housecroft, J. E. Beves, E. L. Dunphy, M. Tomasulo, F. M. Raymo, A. Credi, *Chem. Commun.* **2009**, *12*, 1484–1486; g) S. Silvi, E. C. Constable, C. E. Housecroft, J. E. Beves, E. L. Dunphy, M. Tomasulo, F. M. Raymo, A. Credi, *Chem. Eur. J.* **2009**, *15*, 178–185; h) E. C. Constable, E. L. Dunphy, C. E. Housecroft, W. Kylberg, M. Neuburger, S. Schaffner, E. R. Schofield, C. B. Smith, *Chem. Eur. J.* **2006**, *12*, 4600–4610; i) A. L. Kaledin, Z. Huang, Q. Yin, E. L. Dunphy, E. C. Constable, C. E. Housecroft, Y. V. Geletii, T. Lian, C. L. Hill, D. G. Musaev, *J. Phys. Chem. A* **2010**, *114*, 6284–6297; j) H. Lv, J. A. Rudd, P. F. Zhuk, J. Y. Lee, E. C. Constable, C. E. Housecroft, C. L. Hill, D. G. Musaev, Y. V. Geletii, *RSC Adv.* **2013**, *3*, 20647–20654.
- [6] M. Maestri, N. Armaroli, V. Balzani, E. C. Constable, A. Thompson, *Inorg. Chem.* **1995**, *34*, 2759–2767.
- [7] K. E. Spettel, N. H. Damrauer, *J. Phys. Chem. A* **2014**, *118*, 10649–10662.
- [8] E. C. Constable, M. Devereux, E. L. Dunphy, C. E. Housecroft, J. A. Rudd, J. A. Zampese, *Dalton Trans.* **2011**, *40*, 5505–5515.
- [9] J. Wang, G. S. Hanan, *Synlett* **2005**, *8*, 1251–1254.
- [10] M. J. Frisch, G. W. Trucks, H. B. Schlegel, G. E. Scuseria, M. A. Robb, J. R. Cheeseman, G. Scalmani, V. Barone, G. A. Petersson, H. Nakatsuji, X. Li, M. Caricato, A. V. Marenich, J. Bloino, B. G. Janesko, R. Gomperts, B. Mennucci, H. P. Hratchian, J. V. Ortiz, A. F. Izmaylov, J. L. Sonnenberg, Williams, F. Ding, F. Lipparini, F. Egidi, J. Goings, B. Peng, A. Petrone, T. Henderson, D. Ranasinghe, V. G. Zakrzewski, J. Gao, N. Rega, G. Zheng, W. Liang, M. Hada, M. Ehara, K. Toyota, R. Fukuda, J. Hasegawa, M. Ishida, T. Nakajima, Y. Honda, O. Kitao, H. Nakai, T. Vreven, K. Throssell, J. A. Montgomery Jr., J. E. Peralta, F. Ogliaro, M. J. Bearpark, J. J. Heyd, E. N. Brothers, K. N. Kudin, V. N. Staroverov, T. A. Keith, R. Kobayashi, J. Normand, K. Raghavachari, A. P. Rendell, J. C. Burant, S. S. Iyengar, J. Tomasi, M. Cossi, J. M. Millam, M. Klene, C. Adamo, R. Cammi, J. W. Ochterski, R. L. Martin, K. Morokuma, O. Farkas, J. B. Foresman, D. J. Fox, Wallingford, CT, **2016**.
- [11] C. Adamo, V. Barone, *J. Chem. Phys.* **1999**, *110*, 6158–6170.
- [12] a) T. H. Dunning Jr, P. J. Hay, *Modern Theoretical Chemistry III ed.*, Vol. 3, Plenum, New York, **1977**; b) P. J. Hay, W. R. Wadt, *J. Chem. Phys.* **1985**, *82*, 270–283; c) P. J. Hay, W. R. Wadt, *J. Chem. Phys.* **1985**, *82*, 299–310; d) W. R. Wadt, P. J. Hay, *J. Chem. Phys.* **1985**, *82*, 284–298.
- [13] N. M. O'Boyle, A. L. Tenderholt, K. M. Kangner, *J. Comput. Chem.* **2008**, *29*, 839–845.
- [14] S. Leonid, *V.4.53 2005–2017*, www.chemissian.com.
- [15] M. Cossi, N. Rega, G. Scalmani, V. Barone, *J. Comput. Chem.* **2003**, *24*, 669–681.

Manuscript received: February 3, 2021
Revised manuscript received: June 15, 2021
Accepted manuscript online: June 17, 2021